PAPER

Check for updates

Molecular water oxidation catalysis by zwitterionic carboxylate bridge-functionalized bis-NHC iridium complexes†

Raquel Puerta-Oteo, M. Victoria Jiménez (iD)* and Jesús J. Pérez-Torrente (iD)*

Zwitterionic water-soluble [Cp*Ir^{III}Cl{(MeIm)$_2$CHCOO}] and [Ir^I(cod){(MeIm)$_2$CHCOO}] complexes featuring a carboxylate bridge-functionalized bis-*N*-heterocyclic carbene ligand efficiently catalyzed water oxidation using ammonium cerium(IV) nitrate (CAN) or sodium periodate as sacrificial oxidants. Excellent yields with TOF$_{50}$ numbers up to 1000 h^{-1} have been achieved using CAN as electron acceptor at [CAN]/[Ir] ratios higher than 700. The investigation of the reaction mechanism by UV-vis seems to evidence that both catalyst precursors are transformed into the same active molecular species resulting from the degradation of the hydrocarbon ligands which is partially supported by the similarity of the oxygen evolution profiles at moderate oxidant/catalyst ratios for both catalyst precursors and the same chemical oxidant. In addition, DLS studies provide evidence for the participation of homogeneous iridium molecular species as intermediates likely stabilized by the carboxylate-functionalized bis-NHC ligand.

1. Introduction

The expected energy demand in the medium term, the limited availability of fossil resources and the continuous increase of global CO$_2$ emissions put forward the urgent need for a carbon-neutral renewable energy source. Hydrogen is an energy carrier that is regarded as the fuel of the future due to its high mass-energy density and its clean electrochemical combustion in fuel cells. In this context, water splitting to produce hydrogen and oxygen from water could be a key technological component of a hydrogen economy.[1] Natural photosynthetic processes are an excellent source of inspiration for how to design a catalytic system that can use solar energy for fuel production. Green plants capture sunlight and convert it into energy-rich compounds by oxidation of water and reduction of CO$_2$. However, an artificial photosynthetic system should follow a more practical approach using the solar energy to oxidize H$_2$O to molecular oxygen, as a benign by-product, and then use the generated electrons to reduce protons to molecular hydrogen.[2] Water oxidation is the bottle-neck of this technology since it is a thermodynamically demanding reaction of great molecular complexity from a mechanistic perspective. The oxidation of water to O$_2$ involves the release of 4 H$^+$ and 4 e$^-$ from two water molecules with formation of an oxygen–oxygen bond, thereby requiring both energy and an efficient catalyst.

The development of active and robust water-oxidation catalysts (WOCs) is crucial for the design of artificial photosynthetic devices. A number of transition metal complexes (Mn, Fe, Co, Ni, Ru, Ir, and Cu among others)[3] have been reported as efficient catalysts for water oxidation over the last few years although ruthenium and iridium are among the most active. The assessment of WOCs can be carried out under chemical, electrochemical and photochemical driven conditions.[4] However, from a practical point of view, water oxidation catalysis driven by sacrificial oxidants allows a rapid screening and tuning of the catalysts.[3,5] The use of an electron acceptor, such as CAN or IO$_4^-$, is key in order to re-oxidize the catalysts by removing electrons from the system. Since seminal work by Meyer on the ruthenium "blue dimer" catalyst, the first homogeneous metal-based catalytic system,[6] several ruthenium(II)-based homogeneous water oxidation catalyst are known as the most active molecular catalysts for water oxidation.[7] Later on, Bernhard reported in 2008 the first robust cyclometalated iridium catalyst for water oxidation using CAN as sacrificial oxidant.[8] Thereafter, a series of efficient iridium catalysts featuring an electron rich Cp* ligand in combination with different N^N, N^O, N^C ligands were reported by Crabtree and others as a way to stabilize high-valent iridium intermediates.[9] Further development in the field was the design of robust catalysts based on the powerful electron donating NHC ligands,[10] firstly introduced by Bernhard and Albrecht in 2010,[11] or even bis-NHC ligands

Department of Inorganic Chemistry, Instituto de Síntesis Química y Catálisis Homogénea (ISQCH-CSIC), University of Zaragoza-CSIC, Facultad de Ciencias, C/ Pedro Cerbuna, 12, 50009 Zaragoza, Spain. E-mail: perez@unizar.es

This journal is © The Royal Society of Chemistry 2019

Catal. Sci. Technol., 2019, **9**, 1437–1450 | 1437

taking advantage of the chelate effect.[12] Even so, the number of M-NHC based catalytic systems for water oxidation reactions remains scarce.[13]

Under the harsh reaction conditions, especially when using CAN as oxidant, some hydrocarbon ligands undergo oxidative degradation resulting *in situ* formation of iridium oxide nanoparticles (IrO$_x$) that also catalyse water oxidation. In this context, there has been considerable debate regarding the homogeneous or heterogeneous nature of the catalytic species.[14] Thus, the characterization and identification of catalytic species under turnover conditions is of great importance. The scales of WOC activity are strongly dependent on the nature of the sacrificial oxidant due to the different electron transfer mechanism.[15] In this context, the tendency of NaIO$_4$ to form NPs is negligible compared to CAN thereby avoiding possible complications in the kinetic studies.[10,14a]

Our approach for the design of robust water oxidation catalysts is the use of bis-NHC ligands functionalized with a carboxylate group at the linker.[16] The carboxylate function may confer hemilabile properties to the ligand while imparting water solubility to the complexes. In addition, the potential coordination of the carboxylate to the metal centre might help for the stabilization of high-valent species likely involved in water oxidation catalysis. In this respect, we have recently reported the participation of the dihydrido iridium(III) [Ir^{III}H$_2$(H$_2$O){(MeIm)$_2$CHCOO}], stabilized by the κ^3-C,C',O coordination of the functionalized bis-NHC ligand, in the hydrogenation of CO$_2$ to formate in water catalysed by the zwitterionic iridium(I) [Ir(cod){(MeIm)$_2$CHCOO}] compound.[17]

We report herein on the catalytic activity of zwitterionic water-soluble [Cp*Ir^{III}Cl{(MeIm)$_2$CHCOO}] and [Ir^I-(cod){(MeIm)$_2$CHCOO}] complexes for water oxidation driven by sacrificial oxidants. In addition, kinetic, spectroscopic, electrochemical and mass spectrometry studies have been carried to gain insight into the nature of the catalytic species.

2. Experimental

Synthesis

All the experimental procedures were performed under argon atmosphere by using Schlenk or glovebox techniques. Solvents were taken under argon atmosphere from an Innovative Technologies solvent purification system (SPS), or dried following standard procedures and distilled under argon prior to use.[18] Deuterated solvents CDCl$_3$, CD$_2$Cl$_2$ and DMSO-d_6 (Euriso-top) were dried using activated molecular sieves and degassed by three freeze–pump–thaw cycles. D$_2$O was purchased from Euriso-top and used as received. Standard literature procedures were used to prepare the starting materials [Cp*IrCl$_2$]$_2$ (Cp* = η^5-C$_5$Me$_5$)[19] and [(p-cymene)RuCl$_2$]$_2$.[20] The zwitterionic iridium(III) and rhodium(III) compounds, [Cp*IrCl{(MeIm)$_2$-CHCOO}] (1) and [Cp*RhCl{(MeIm)$_2$CHCOO}] (2), complex [Cp*IrCl{(MeIm)$_2$CHCOOMe}]OTf (3),[16] and zwitterionic iridium(I) compound [Ir(cod){(MeIm)$_2$CHCOO}] (4)[17] were prepared following the procedure recently reported by us.

Scientific equipment

^{1}H and ^{13}C{^{1}H} NMR spectra were recorded on Bruker Avance spectrometers (300, 400 or 500). Chemical shifts are reported in ppm relative to tetramethylsilane and coupling constants (*J*) are given in Hertz (Hz). Spectral assignments were performed, when necessary, with the help of 2D-NMR experiments. Electrospray ionization (ESI) mass spectra were recorded using a Bruker Esquire3000 plus™ ion-trap mass spectrometer equipped with a standard ESI source. High-resolution electrospray ionization mass spectra (HRMS-ESI) were recorded using a Bruker MicroToF-Q™ equipped with an API-ESI source and a Q-ToF mass analyzer. Infrared spectra were recorded on a 100 FTIR-Perkin-Elmer Spectrophotometer equipped with a universal attenuated total reflectance (UATR) accessory made by thallium bromide–iodide crystals (KRS-5). C, H and N analyses were carried out in a Perkin-Elmer 2400 Series II CHNS/O analyzer. The UV/vis spectra were recorded on a JASCO UV-vis-NIR V-670 spectrophotometer equipped with a single monochromator that covers a wavelength range from 190 to 2500 nm. Dynamic light scattering studies were carried out on a Malvern Zetasizer Nano ZS which measures the diffusion of particles moving under Brownian motion, and converts this to size and size distribution using Stokes–Einstein relationship. This device incorporates non-invasive back scatter technology (NIBS) to give the highest sensitivity simultaneously with the highest size and concentrations range in a measurement range from 0.3 nm to 10.0 microns (diameter). Electrochemical experiments were performed on a potentiostat EG&G Research Model 273. The electrochemical cell is equipped with a three electrode system: platinum disk as a working electrode, platinum thread as auxiliary electrode and a saturated calomel electrode (SCE, saturated with KCl) as a reference electrode. Electrochemical experiments were carried out under argon in about 5 × 10^{-4} M of the complexes and 0.1 M in tetrabutylammonium hexafluorophosphate, [N(n-Bu)$_4$]PF$_6$ (TBAH), or sodium tetrafluoroborate, NaBF$_4$, in the potential range +1.8 to −1.8 (H$_2$O) at variable scan rates. The measurements were performed at room temperature and the adjustments of pH were made *via* addition of HNO$_3$. Redox potentials were referenced in acetonitrile to the Fc/Fc$^+$ couple (0.43 V for SCE as reference electrode).

Synthesis of the complexes

Synthesis of [(p-cymene)RuCl{(MeIm)$_2$CHCOO}] (5). [(p-Cymene)RuCl$_2$]$_2$ (124.9 mg, 0.204 mmol) was added to a solution of [(MeIm)$_2$CHCOOAg]$_2$ (133.5 mg, 0.204 mmol) in CH$_2$Cl$_2$/MeOH (10 mL, 1:1, v:v) in the absence of light. The suspension was stirred for 6 hours and then filtered *via* a cannula through Celite to remove the AgCl formed. Then, the resulting solution was concentrated to *ca.* 1 mL under reduced pressure. Slow addition of diethyl ether afforded the compound as an orange solid which was filtered, washed with diethyl ether (3 × 3 mL) and dried *in vacuo*. Yield: 143.9 mg, 72%. Anal. calc. for C$_{20}$H$_{25}$ClN$_4$O$_2$Ru: C 49.03; H, 5.14; N,

1438 | *Catal. Sci. Technol.*, 2019, **9**, 1437–1450

This journal is © The Royal Society of Chemistry 2019

11.43. Found: C, 49.25; H, 5.18; N, 11.59. ^{1}H NMR (298 K, 300 MHz, CDCl$_3$): δ 7.90 (d, J_{H-H} = 1.9, 2H, CH), 6.96 (d, J_{H-H} = 1.9, 2H, CH), 5.63 (s, 1H, CHCOO), 5.61 (d, J_{H-H} = 6.2, 2H, =CH p-cym), 5.47 (d, J_{H-H} = 6.2, 2H, =CH p-cym), 3.97 (s, 6H, NCH$_3$), 2.38 (spt, J_{H-H} = 6.8, 1H, CH, ^{i}Pr p-cym), 2.22 (s, 3H, CH$_3$, p-cym), 1.01 (d, J_{H-H} = 6.8, 6H, CH$_3$, ^{i}Pr p-cym). ^{13}C{^{1}H} NMR (298 K, 75 MHz, CDCl$_3$): δ 174.2 (C$_{NCN}$), 163.5 (COO), 122.7, 122.3 (CH), 107.6 (C-^{i}Pr, p-cym), 104.6 (C-Me, p-cym), 92.4 (CH, p-cym), 85.5 (CH, p-cym), 75.0 (CHCOO), 38.2 (NCH$_3$), 32.2 (CH, ^{i}Pr p-cym), 22.9 (CH$_3$, p-cym), 18.8 (CH$_3$, ^{i}Pr p-cym). MS (ESI$^+$, CH$_2$Cl$_2$/MeOH, m/z, %): 491.1 ([M + H]$^+$, 100). IR (ATR, cm^{-1}): 1654 (COO).

Synthesis of 1,1′-bis(N-butylimidazole)acetate bromide, [(n-BuImH)$_2$CHCOO]Br. Ethyl dibromoacetate (0.5 mL, ρ = 1.902 g mL^{-1}, 3.86 mmol) and 1-(n-butyl)imidazole (1.0 mL, ρ = 0.945 g mL^{-1}, 7.61 mmol) were dissolved in THF (4 mL) into a Teflon-sealed glass vessel and the solution stirred at 343 K for 72 hours. After cooling to room temperature the brown solid residue was dissolved in methanol and the solution concentrated to $ca.$ 5 mL. Addition of acetone (10 mL) gave the salt as a white solid that was filtered, washed with acetone (3 × 10 mL) and dried under vacuum. Yield: 952.0 mg, 64%. Anal. calc. for C$_{16}$H$_{25}$BrN$_4$O$_2$: C, 49.88; H, 6.54; N, 14.54. Found: C, 49.57; H, 6.57; N, 14.48. ^{1}H NMR (298 K, 300 MHz, DMSO-d_6): δ 9.57 (t, J_{H-H} = 1.7, 2H, NCHN), 7.97 (t, J_{H-H} = 1.7, 2H, CH), 7.86 (t, J_{H-H} = 1.7, 2H, CH), 7.15 (s, 1H, CHCOO), 4.22 (t, J_{H-H} = 7.3, 4H, NCH$_2$), 1.79 (m, J_{H-H} = 7.4, 4H, CH$_2$), 1.27 (m, J_{H-H} = 7.3, 4H, CH$_2$), 0.90 (t, J_{H-H} = 7.3, 6H, CH$_3$). ^{13}C{^{1}H} NMR (298 K, 75 MHz, DMSO-d_6): δ 159.4 (COO), 137.4 (C$_{NCN}$), 122.3, 122.2 (CH), 70.6 (CHCOO), 48.9 (CH$_2$-Im), 31.1 (CH$_2$), 18.8 (CH$_2$), 13.3 (CH$_3$). MS (ESI$^+$, MeOH, m/z, %): 261.2 ([M-COO]$^+$, 100). IR (ATR, cm^{-1}): 1670 (COO).

Synthesis of [(n-BuIm)$_2$CHCOOAg]$_2$. Ag$_2$O (125.2 mg, 0.540 mmol) was added to a white suspension of [(n-BuImH)$_2$CHCOO]Br (208.1 mg, 0.540 mmol) in CH$_2$Cl$_2$ (5 mL) and the mixture refluxed for 24 hours in the dark. The solution was filtered via cannula through Celite and concentrated under vacuum to give a white suspension which was decanted. The white precipitate was washed with diethyl ether and dried under vacuum. Yield: 182.1 mg, 82%. Anal. calc. for C$_{32}$H$_{46}$Ag$_2$N$_8$O$_4$: C, 46.73; H, 5.64; N, 13.62. Found: C, 46.65; H, 5.62; N, 12.59. ^{1}H NMR (298 K, 300 MHz, CD$_2$Cl$_2$): δ 7.76 (s, 4H, CH), 7.13 (s, 2H, CHCOO), 7.03 (s, 4H, CH), 4.06 (m, J_{H-H} = 7.3, 8H, NCH$_2$), 1.88–1.68 (m, J_{H-H} = 7.3, 8H, CH$_2$), 1.33 (m, J_{H-H} = 7.3, 8H, CH$_2$), 0.92 (t, J_{H-H} = 7.3, 12H, CH$_3$). MS (ESI$^+$, CH$_2$Cl$_2$/MeOH, m/z, %): 822.2 ([M], 74), 778.9 ([M-COO]$^+$, 26), 735.0 ([M-2COO]$^+$, 100). IR (ATR, cm^{-1}): 1667 (COO).

Synthesis of [Cp*IrCl{(n-BuIm)$_2$CHCOO}] (6). [Cp*IrCl$_2$]$_2$ (59.6 mg, 0.075 mmol) was added to a solution of [(n-BuIm)$_2$CHCOOAg]$_2$ (61.5 mg, 0.075 mmol) in CH$_2$Cl$_2$/MeOH (10 mL, 1:1, v:v) in the absence of light. The suspension was stirred for 6 hours and then filtered via a cannula through Celite to remove the AgCl formed. Then, the resulting solution was concentrated to $ca.$ 1 mL under reduced pressure. Slow addition of diethyl ether afforded the compound as a pale yellow solid which was filtered, washed

with diethyl ether (3 × 3 mL) and dried in $vacuo$. Yield: 82.9 mg, 83%. Anal. calc. for C$_{26}$H$_{38}$ClIrN$_4$O$_2$: C 46.87; H, 5.75; N, 8.41. Found: C, 46.74; H, 5.71; N, 8.68. ^{1}H NMR (298 K, 300 MHz, CD$_2$Cl$_2$): δ 7.80 (d, J_{H-H} = 2.2, 2H, CH), 7.05 (d, J_{H-H} = 2.2, 2H, CH), 5.70 (s, 1H, CHCOO), 4.25 (br m, 4H, NCH$_2$), 3.79 (br m, 4H, CH$_2$), 1.76 (s, 15H, CH$_3$ Cp*), 1.42 (dq, J_{H-H} = 14.7, 7.4, 4H, CH$_2$), 0.97 (t, J_{H-H} = 7.4, 6H, CH$_3$). ^{13}C{^{1}H} NMR (298 K, 75 MHz, CD$_2$Cl$_2$): δ 163.7 (COO), 151.2 (C$_{NCN}$), 122.7, 120.1 (CH), 93.3 (CCH$_3$ Cp*), 75.6 (CHCOO), 50.4 (NCH$_2$), 20.7 (2C, CH$_2$), 14.2 (CH$_3$), 9.8 (CH$_3$ Cp*). MS (ESI$^+$, CH$_2$Cl$_2$/MeOH, m/z, %): 667.2 ([M + H]$^+$, 100). IR (ATR, cm^{-1}): 1659 (COO).

Synthesis of [Cp*IrI{(MeIm)$_2$CH$_2$}]PF$_6$ (7). The compound was prepared following a modified procedure of that described by Heinekey and co-workers.[21] AgPF$_6$ (209.2 mg, 0.827 mmol) was added to a solution of [Cp*IrCl$_2$]$_2$ (164.9 mg, 0.207 mmol) in acetonitrile (5 mL) and the mixture stirred for 4 hours at room temperature. The resulting yellow suspension was filtered through Celite to remove the silver salt to give a yellow solution. The addition of [(MeImH)$_2$CH$_2$]I$_2$ (178.9 mg, 0.414 mmol) gave an orange suspension which turned into red whereupon the addition of NEt$_3$ (116.0 μL, ρ = 0.726 g mL^{-1}, 99.5%, 0.828 mmol). The red suspension was heated at 333 K for 48 h to give a dark orange solution. The solution was cooled to room temperature and the solvent removed under vacuum. The addition of CHCl$_3$ (5 mL) resulted in a yellow suspension which was decanted and then filtered. The yellow solid was washed with methanol (2 × 5 mL) and diethyl ether (3 × 3 mL), and dried in $vacuo$. Yield: 244.0 mg, 76%. ^{1}H NMR (298 K, 300 MHz, CD$_2$Cl$_2$): δ 7.39 (d, J_{H-H} = 2.1, 2H, CH), 7.17 (d, J_{H-H} = 2.1, 2H, CH), 6.16 (d, J_{H-H} = 13.2, 1H, NCH$_2$N), 5.70 (d, J_{H-H} = 13.2, 1H, NCH$_2$N), 3.81 (s, 6H, NCH$_3$), 1.97 (s, 15H, CH$_3$ Cp*).

Reaction of [Ir(cod){(MeIm)$_2$CHCOO}] (4) with NaIO$_4$. An NMR tube was charged with a solution of 4 (15.3 mg, 0.030 mmol) in D$_2$O (0.5 mL). Addition of solid NaIO$_4$ (7.70 mg, 0.036 mmol) resulted in the formation of a green solution of [Ir(OD)(cod){(MeIm)$_2$CHCOO}]$^+$ (d-8). NNR data: ^{1}H NMR (298 K, 300 MHz, D$_2$O): δ 7.63 (d, J_{H-H} = 1.9, 2H, CH), 7.25 (d, J_{H-H} = 1.9, 2H, CH), 6.84 (s, 1H, CHCOO), 6.63 (m, 2H, =CH cod), 5.96 (m, 2H, =CH cod), 4.04 (s, 6H, NCH$_3$), 2.75 (m, 2H, >CH$_2$ cod), 2.59 (m, 2H, >CH$_2$ cod), 2.44 (m, 4H, >CH$_2$ cod).

Reaction of [Ir(cod){(MeIm)$_2$CHCOO}] (4) with CAN. An NMR tube was charged with a solution of compound 4 (15.3 mg, 0.030 mmol) in D$_2$O (0.5 mL). Addition of variable amounts of solid CAN allowed the identification of the following species: NMR data for [IrD(cod){(MeIm)$_2$CHCOO}]$^+$ (d-9). ^{1}H NMR (298 K, 300 MHz, D$_2$O): δ 7.57 (d, J_{H-H} = 1.8, 2H, CH), 7.17 (d, J_{H-H} = 1.8, 2H, CH), 6.75 (s, 1H, CHCOO), 6.02 (m, 2H, =CH cod), 4.81 (m, 2H, =CH cod), 3.80 (s, 6H, NCH$_3$), 2.75 (m, 4H, >CH$_2$ cod), 2.55 (m, 2H, >CH$_2$ cod), 2.38 (m, 2H, >CH$_2$ cod).

NMR data for [Ir(D$_2$O)(cod){(MeIm)$_2$CHCOO}]$^{2+}$ (d$_2$-10). ^{1}H NMR (298 K, 300 MHz, D$_2$O): δ 7.66 (d, J_{H-H} = 1.7, 2H, CH), 7.26 (d, J_{H-H} = 1.7, 2H, CH), 6.91 (s, 1H, CHCOO), 6.84 (m, 2H, =CH cod), 5.89 (m, 2H, =CH cod), 4.00 (s, 6H, NCH$_3$),

3.03 (m, 2H, >CH_2 cod), 2.56 (m, 2H, >CH_2 cod), 2.43 (m, 4H, >CH_2 cod).

Synthesis of [Ir(OH)(cod){(MeIm)$_2$CHCOO}][IO$_3$] (8). Solid $NaIO_4$ (20.53 mg, 0.096 mmol) was added to a red solution of **4** (50.0 mg, 0.096 mmol) in H_2O (1 mL) and stirred for 15 minutes to give a light green solution. The solvent was evaporated almost dryness to give a white suspension. The precipitation was completed by addition of methanol (1 mL). The white precipitate was washed with methanol and dried under vacuum. Yield: 43 mg, 63%. ^1H NMR (298 K, 300 MHz, D_2O): δ 7.63 (d, J_{H-H} = 1.9, 2H, CH), 7.25 (d, J_{H-H} = 1.9, 2H, CH), 6.84 (s, 1H, CHCOO), 6.63 (m, 2H, =CH cod), 5.96 (m, 2H, =CH cod), 4.02 (s, 6H, NCH_3), 2.74 (m, 2H, >CH_2 cod), 2.58 (m, 2H, >CH_2 cod), 2.44 (m, 4H, >CH_2 cod) (OH not observed due to H/D exchange). $^{13}C\{^1H\}$ NMR (298 K, 75 MHz, D_2O): δ 168.09 (COO), 138.31 (C_{NCN}), 125.86, 121.59 (CH), 115.88, 114.85 (=CH cod), 72.60 (CHCOO), 36.87 (NCH_3), 28.52, 28.40 (>CH_2 cod). MS (HRESI$^+$, CH_3CN/H_2O, m/z, %): 537.1491 ([M]$^+$, 100), 515.1382 ([M−OH−H]$^+$, 67). IR (ATR, cm^{-1}): 3391 (OH), 1633 (COO), 787, 767, 724 (IO_3^-).

Synthesis of [Ir(H$_2$O)(cod){(MeIm)$_2$CHCOO}]X$_2$ (X = IO$_3$/ NO$_3$) (10). HNO_3 (19.4 μL, ρ = 1.395 g mL^{-1}, 0.028 mmol) was slowly added to a suspension of **8** (20.0 mg, 0.028 mmol) in H_2O (1 mL) and left stirring for 5 minutes. The solution was carried to dryness to give a white solid which was washed with methanol (2 × 0.5 mL) and dried under vacuum. Yield: 10 mg, 45%. ^1H NMR (298 K, 300 MHz, D_2O): δ 7.66 (d, J_{H-H} = 2.1, 2H, CH), 7.29 (d, J_{H-H} = 2.1, 2H, CH), 6.94 (s, 1H, CHCOO), 6.89 (m, 2H, =CH cod), 6.23 (m, 2H, =CH cod), 3.89 (s, 6H, NCH_3), 2.91 (m, 2H, >CH_2 cod), 2.50 (m, 2H, >CH_2 cod), 2.41 (m, 4H, >CH_2 cod). (HRESI$^+$, H_2O, m/z, %): 599.0501 ([M + NO_3]$^+$, 57), 537.1477 ([M − H]$^+$, 89), 519.1379 ([M-H_3O]$^+$, 79).

General procedure for catalytic water oxidation

The reactions were performed on a *Man on the Moon* series X102 kit micro-reactor[22] with a total volume of 14.2 mL placed in a thermostatic water bath at 298 K. The reaction vessel is connected to a switchable 3-way valve *via* a Thorion screw through polyamide tubing. The valve can be switched between two positions, one of them connecting the reactor vessel to the exterior so that it can be used like a conventional Schlenk flask. The other position connects the flask to the pressure transducer which allows for the measurement of $O_2(g)$ evolution. A 2 mL water-solution of the sacrificial oxidant CAN (0.354 M, pH = 1) or $NaIO_4$ (0.193 M, pH = 6–7) was placed in the glass reactor under argon atmosphere. The reactor was closed, thermally equilibrated at 298 K and then, the pressure measurement started. Once the pressure was stabilized, 0.5 mL water-solution of the catalyst was injected. Oxygen evolution was measured until constant pressure and the amount of $O_2(g)$ (mmol) produced was calculated by using the ideal gas law. Each value is averaged out form three measurements with reproducibility better than ±1%.

Multi-step water oxidation reactions were performed by sequential addition of 2 mL of a solution of CAN (0.354 M, pH = 1). The first measurement was performed following the experimental procedure described above using a [CAN]/[Ir] ratio of 700. Once stable pressure of $O_2(g)$ was achieved, the pressure inside the micro-reactor was released and another 2 mL of CAN (0.354 M) were added over the remaining dark purple solution. The measurement starts as prompt as the fresh CAN solution is injected and continues until constant pressure. The space inside the micro-reactor (14.2 mL) and the total volume of solution placed inside limited the number of additions to a maximum of three.

3. Results and discussion

The potential as catalysts for water oxidation of selected water-soluble iridium, rhodium and ruthenium zwitterionic complexes: [Cp*IrCl{(MeIm)$_2$CHCOO}] (**1**), [Cp*RhCl{(MeIm)$_2$-CHCOO}] (**2**) and [(*p*-cymene)RuCl{(MeIm)$_2$CHCOO}] (**5**), was screened in preliminary tests. A few milligrams of each zwitterionic complex was added into a vial and dissolved in 3 mL of degassed Milli-Q water. Subsequent addition of a large excess of solid CAN or $NaIO_4$ resulted in the vigorous formation of bubbles due to oxygen evolution for the iridium precursor **1**. However, no reaction was observed for the rhodium precursor **2**, and just a few oxygen bubbles were observed for the ruthenium precursor **5**. The colour of the solution after oxygen evolution remains purple and fades after 30 min when using CAN as chemical oxidant. However, a colour change from deep green to blue was observed with $NaIO_4$ (see ESI†). These qualitative tests prompted us to study the catalytic activity not only of [Cp*IrCl{(MeIm)$_2$CHCOO}] (**1**) but also of the related zwitterionic iridium(I) complex [Ir(cod){(MeIm)$_2$-CHCOO}] (**4**) featuring a 1,5-cyclooctadiene ligand (Chart 1).

Catalytic activity of Ir(bis-NHC) complexes for water oxidation driven by CAN and $NaIO_4$

Water oxidation catalytic reactions were performed under argon atmosphere on a micro-reactor equipped with a pressure transducer that allows the measurement of $O_2(g)$ evolution. The catalytic tests were performed in acidic-buffered degassed water (0.1 M HNO_3, pH = 1) using a fixed amount of CAN (0.283 M) varying the concentration of catalyst precursors **1** or **4** in a range from 80 to 2820 μM. Table 1 summarizes the
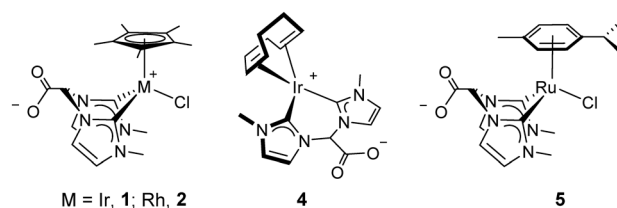

Chart 1 Selected iridium, rhodium and ruthenium zwitterionic complexes as catalyst precursors for water oxidation.
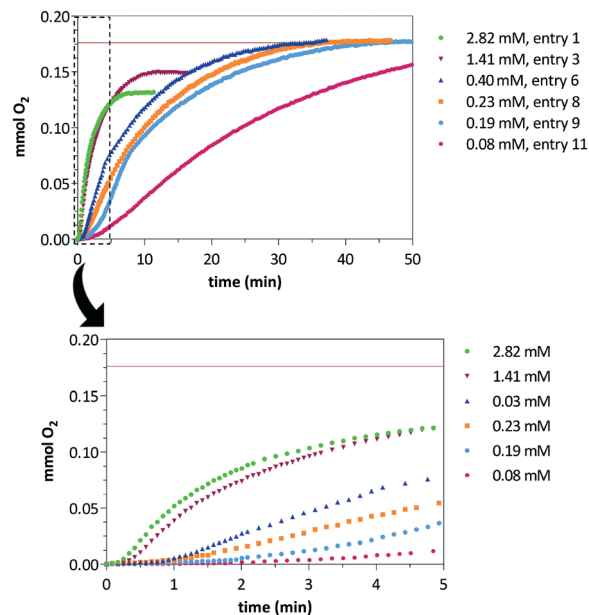
1440 | *Catal. Sci. Technol.*, 2019, **9**, 1437–1450

This journal is © The Royal Society of Chemistry 2019

Table 1 Influence of the [CAN]/[Ir] ratio in CAN-driven water oxidation catalyzed by **1** and **4**[a]

Cat.	$[Ir]^b$	$[Ce^{IV}]/[Ir]$	mmol O_2	TON	$TOF_{50}{}^c$	Yield (%)
1	2.82	100	0.132	19	380	74
1	2.34	120	0.136	23	380	77
1	1.41	200	0.150	42	600	85
1	0.94	300	0.157	67	630	89
1	0.47	600	0.166	142	850	94
1	0.40	700	0.172	178	950	97
1	0.35	800	0.174	199	840	99
1	0.23	1200	0.177	308	1080	>99
1	0.19	1500	0.177	375	1000	>99
1	0.15	1900	0.177	471	1040	>99
1	0.08	3700	0.175	891	1300	99
4	2.82	100	0.146	21	250	82
4	0.40	700	0.174	174	730	98
4	0.19	1500	0.170	357	900	96

[a] Catalysts: [Cp*IrCl{(MeIm)$_2$CHCOO}] (**1**) and [Ir(cod){(MeIm)$_2$CHCOO}] (**4**). Reactions were carried out in 2.5 mL of acid-buffered degassed water (0.1 M HNO$_3$, pH = 1) in a thermostatic bath at 300 K at indicated [CAN]/[Ir] ratios, $[CAN]_0$ = 0.283 M. [b] [Ir] mM. [c] Turnover frequency (h^{-1}) calculated at reaction time when the number of mmol of produced O$_2$(g) reached half of the theoretically calculated.

Fig. 1 Plot of mmol of O$_2$(g) *vs.* time at various concentrations of complex [Cp*IrCl{(MeIm)$_2$CHCOO}] (**1**) with enlarged plots of the boxed region showing the oxygen evolution at short reaction times. The produced oxygen in all the catalytic tests is consistent with the stoichiometric limit of added CAN (horizontal line).

CAN-driven water oxidation catalytic experiments including the number of mmol of produced O$_2$(g), TON number expressed as mmol of O$_2$(g) per mmol of catalyst, and TOF$_{50}$. The maximum amount of produced O$_2$(g) under these experimental conditions is 0.177 mmol. Remarkably, an increase of the reaction yield was observed by reducing the catalyst concentration. Although roughly a 75% yield was achieved with a [CAN]/[Ir] ratio of 100 for catalyst **1** (entry 1), almost full conversion was attained when using ratios higher than 700 at longer reaction times (entries 6 to 11). The increase of the catalyst concentration resulted in faster reactions although the oxygen evolution stops before reaching the maximum conversion (entries 1 to 5) as was evidenced by the plateau in the O$_2$(g) evolution plot (Fig. 1).[23] However, these solutions showed catalytic activity after successive CAN additions once oxygen evolution stops which points to a likely Ir/Ce dinuclear resting state of the catalyst that becomes activated upon addition of an excess of CAN.[9b,24] An induction period of 0.3–2.0 minutes was found before the O$_2$(g) formation initiates which might be associated to the generation of active high-valent

iridium species (Fig. 1, bottom). In line with these results, increasing the concentration of catalyst precursor **4** resulted in faster O$_2$(g) evolution but the maximum yield (0.177 mmol) was not reached either. Similarly, full conversion was attained at higher [CAN]/[Ir] ratios although longer reaction times were required (entries 12–14, Table 1). The observed lag phases for **4** are roughly one minute longer than those observed for **1** at the same [CAN]/[Ir] ratio (see ESI†).

The catalytic activity of both iridium precursors was also studied using NaIO$_4$ as sacrificial oxidant. The reactions were carried out in degassed Milli-Q water using a fixed amount of NaIO$_4$ (0.154 M) in a range of catalyst concentrations from 150 to 1540 μM. Under these reaction conditions the pH of the solution is approximately 7.0 and it does not change appreciably over the course of the reaction. The performed NaIO$_4$-driven water oxidation catalytic experiments are summarized in Table 2.

Table 2 Influence of the [NaIO$_4$]/[Ir] ratio in NaIO$_4$-driven catalytic water oxidation by complexes **1** and **4**[a]

Entry	Cat.	$[Ir]^b$	$[NaIO_4]/[Ir]$	mmol O_2	TON	$TOF_{50}{}^c$	Yield (%)
1	1	1.54	100	0.178	46	160	92
2	1	0.51	300	0.158	124	120	82
3	1	0.15	1000	0.167	445	284	86
4	4	1.54	100	0.178	46	120	92
5	4	0.51	300	0.159	125	105	82
6	4	0.15	1000	0.163	435	285	84

[a] Catalysts: [Cp*IrCl{(MeIm)$_2$CHCOO}] (**1**) and [Ir(cod){(MeIm)$_2$CHCOO}] (**4**). Reactions were carried out in 2.5 mL of degassed water (pH = 7) in a thermostatic bath at 300 K at indicated [NaIO$_4$]/[Ir] ratios, $[NaIO_4]_0$ = 0.154 M. [b] [Ir] mM. [c] Turnover frequency (h^{-1}) calculated at reaction time when the number of mmol of produced O$_2$(g) reached half of the theoretically calculated.
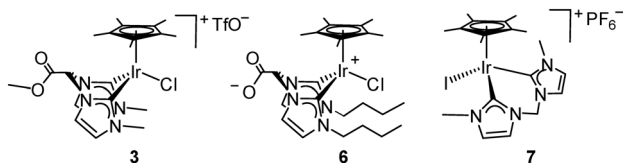
Fig. 2 Selected Cp*Ir(bis-NHC) compounds as catalyst for water oxidation.

Inspection of the $O_2(g)$ vs. time plots showed induction periods of 2–3 min for 1 and 3–4 min for 4 (see ESI†). Although high yields were achieved regardless of the catalyst concentration, the amount of $O_2(g)$ produced in all cases was below the theoretical maximum yield (0.192 mmol). From these results, it becomes evident that the generation of the catalytic active species is faster when CAN is used as sacrificial oxidant.[25] The $O_2(g)$ evolution is also faster with CAN, as evidenced by the attained TOF_{50} values at similar catalyst concentration.

In order to explore the influence of the alkyl-wingtip and the carboxylate functional group at the bis-NHC ligand on the catalyst performance in water oxidation, the catalytic activity of complexes [Cp*IrCl{(MeIm)$_2$CHCOOMe}]OTf (3), [Cp*IrCl{(n-BuIm)$_2$CHCOO}] (6) and [Cp*IrI{(MeIm)$_2$CH$_2$}]PF$_6$ (7) has been evaluated (Fig. 2).

As can be seen in Table 3, the three selected catalysts were found to be less active than 1 at a [NaIO$_4$]/[Ir] ratio of 100 (entries 1–4). In terms of the amount of produced $O_2(g)$, the catalytic performance of 6, featuring n-butyl wingtips, is very similar to 1 with a 93% yield, which is in agreement with their closely related structure. However, lower yields were attained with catalysts 3 (featuring a methoxycarbonyl functional group) and 7 (lacking a carboxylate group), 83 and 73%, respectively, which points to a positive effect of the carboxylate functionality in the stabilization of the active species. Similar results have been obtained using CAN as sacrificial oxidant at a [CAN]/[Ir] ratio of 100 (entries 5–8) with 1 as the most active catalyst with a TOF_{50} of 385 h^{-1}. Macchioni et al. described the positive influence of a long alkyl chain wingtip (methyl vs. n-octyl) in the ancillary NHC ligand of Cp*Ir(NHC)-based catalysts in water oxidation driven by

CAN.[25] The presence of n-butyl substituents in 6 does not improve the catalytic activity and the observed TOF_{50} values were significantly lower than those attained with catalyst 1 also using a high [CAN]/[Ir] ratio of 1200 (entries 9 and 10).

As can be inferred for the activity data, catalyst precursor 1 is slightly more active than 4, both showing an average activity in the range of many of the iridium complexes so far reported. Their activity is comparable to those shown by the pyridine–dicarboxylate complex, [IrCp*Cl{2,6-Py(COO)-(COOH)}],[26] and the solvato complex [Cp*Ir(H$_2$O)$_3$](NO$_3$)$_2$,[27] with TOF_{50} values of 1380 h^{-1} and 1260 h^{-1}, respectively; and is superior to that of [Cp*Ir(H$_2$O)(5,5′-Me-bipy)]$^+$ with 576 h^{-1}.[28] In addition, both complexes are more active than related bis-NHC [Cp*IrCl{(MeIm)$_2$CH$_2$}]PF$_6$[29] and [Cp*IrCl{(MeIm)$_2$(CH$_2$)$_2$}]PF$_6$[30] complexes, with TOF_{50} of 432 h^{-1} and 720 h^{-1}, respectively, and the Cp*Ir-mesoionic triazolylidene-pyridine with 960 h^{-1}.[25] On the other hand, the activities of our complexes are far away from that shown by [IrCp*(H$_2$O)(3,3′-OH-bipy)]$^+$ or [IrCp*(H$_2$O)(3,3′-OH-bipym)]$^+$, with outstanding TOF_{50} numbers of 13 500 h^{-1} and 18 720 h^{-1}, respectively.[31]

Kinetic studies

With the aim of shed some light on the operating mechanism in our catalytic systems, we have carried out kinetic investigations on the CAN- and NaIO$_4$-driven water oxidation catalyzed by 1 and 4. Regardless of the catalyst concentration, the highest rate of $O_2(g)$ evolution was observed at roughly 20% conversion of the sacrificial oxidant with [CAN]$_0$ = 0.283 M and [NaIO$_4$]$_0$ = 0.154 M. Thus, the reaction times required to reach 20% conversion were extracted from the $O_2(g)$ evolution vs. time plots and used to determine the maximum oxygen evolution rate (μmol min^{-1}) for each catalyst concentration. The maximum rate of oxygen evolution vs. catalyst concentration plot for the catalytic system 1/CAN is shown in Fig. 3a. The plot shows a linear relationship although a significant departure from linearity was observed at high catalyst concentrations. This linear relationship has been previously observed for related iridium-based WOCs using CAN as sacrificial oxidant.[23,32] The slope of the plots for 1 and 4 with

Table 3 Water oxidation by Cp*Ir(bis-NHC) complexes driven by NaIO$_4$ or CAN as sacrificial oxidants[a]

Entry	Cat.	[Ir][b]	Oxid.	[oxid]/[Ir]	mmol O_2	TON	TOF_{50}[c]	Yield (%)
1	1	1.54	NaIO$_4$	100	0.178	46	170	92
2	3	1.54	NaIO$_4$	100	0.160	42	115	83
3	6	1.54	NaIO$_4$	100	0.179	46	110	93
4	7	1.54	NaIO$_4$	100	0.140	36	140	73
5	1	2.82	CAN	100	0.132	19	385	74
6	3	2.82	CAN	100	0.149	21	265	84
7	6	2.82	CAN	100	0.114	20	85	64
8	7	2.82	CAN	100	0.143	20	175	81
9	1	0.23	CAN	1200[c]	0.177	308	1080	>99
10	6	0.23	CAN	1200[c]	0.153	266	425	86

[a] Reactions were carried out in 2.5 mL degassed water (pH = 7.0) at 300 K, [NaIO$_4$]$_0$ = 0.154 M (pH = 7.0) or [CAN]$_0$ = 0.282 M (0.1 M HNO$_3$, pH = 1). [b] [Ir] mM. [c] Turnover frequency (h^{-1}) calculated at reaction time of 50% of theoretically calculated $O_2(g)$.
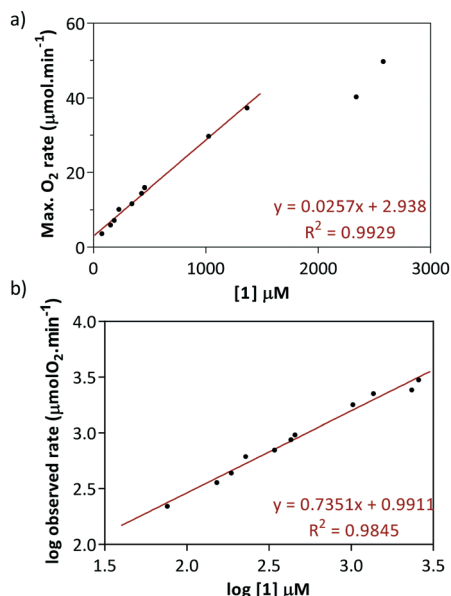
1442 | Catal. Sci. Technol., 2019, 9, 1437–1450

This journal is © The Royal Society of Chemistry 2019

a) Plot with y-axis "Max. O$_2$ rate (μmol.min^{-1})" and x-axis "[1] μM"

$y = 0.0257x + 2.938$
$R^2 = 0.9929$

b) Plot with y-axis "log observed rate (μmolO$_2$.min^{-1})" and x-axis "log [1] μM"

$y = 0.7351x + 0.9911$
$R^2 = 0.9845$

Fig. 3 a) Plot of maximum rate of O$_2$(g) evolution determined at 20% conversion of CAN vs. concentration of catalyst [Cp* IrCl{(MeIm)$_2$CHCOO}] (**1**). b) Log(rate)–log[**1**] plot and the corresponding linear fit.

both sacrificial oxidants evidences the faster rate of oxygen evolution for CAN with both catalyst precursors. Furthermore, oxygen-evolution rate is also faster for catalyst **1** with both sacrificial oxidants (see ESI†). The activity values for the catalytic systems **1**/CAN and **4**/CAN (2.82–0.19 mM) are in the range of 8–19 and 2–9 TON min^{-1}, respectively.

The log–log plot of the maximum oxygen evolving rate against catalyst concentration provides information about the reaction order in catalyst.[33] Water oxidation performed with catalyst **1** driven by NaIO$_4$ seems to proceed via apparent first-order kinetics (reaction order of 1.1) whilst complex **4** exhibits a reaction order of 0.7 under the same reaction conditions.[32] A broken order was also observed for water oxidation processes driven by CAN, 0.7 for complex **1** (Fig. 3b) and 0.5 for complex **4** (see ESI†). Studies with several iridium-based catalysts also reported a fractional order dependence on the catalyst, which evidences the complexity of water oxidation reactions from the kinetic and mechanism viewpoint.[23,27,32,34]

The interpretation of the kinetic data with NaIO$_4$ as oxidant entails extra difficulties since oxygen evolution could also result from decomposition of IO$_4^-$ rather than water oxidation by the iridium catalyst.[14f] Therefore, the effect of the sacrificial oxidant concentration on water oxidation catalysis has been studied with CAN. The kinetics of CAN-driven water oxidation by catalyst **1** was studied by varying the CAN concentration from 46 to 503 mM at a fixed catalyst concentration of 182 μM. The highest rate of oxygen evolution, determined at 20% of CAN conversion, was observed at 92 mM of CAN with a value of 7.32 μmol min^{-1} (Fig. 4). A gradual decrease was observed at higher CAN concentrations, reaching a value as low as 4.18 μmol min^{-1} for a CAN concentration of

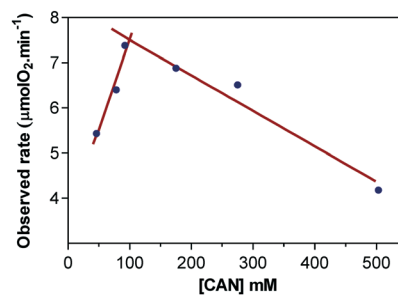Plot with y-axis "Observed rate (μmolO$_2$.min^{-1})" and x-axis "[CAN] mM"

Fig. 4 Variation of the maximum rate of O$_2$(g) evolution rate (determined at 20% conversion of CAN) versus concentration of CAN at a fixed 182 μM concentration of catalyst precursor [Cp* IrCl{(MeIm)$_2$CHCOO}] (**1**).

503 mM. It seems that the initial linear increase of the rate of maximum oxygen evolution was attributed to a first order dependence on CAN, and the decay of the rate of maximum oxygen evolution at high CAN concentrations has been attributed to an increase of the ionic strength of the catalytic solution or aggregation of cerium(IV) into dimeric species.[35]

In order to test whether the purple solutions obtained after CAN-driven water oxidation catalysis have the potential to restart its catalytic activity, O$_2$(g) evolution was monitored during the step-wise addition of aqueous CAN solution (pH = 1.0) to a water solution of catalyst **1**. Fig. 5 shows the plot of O$_2$(g) evolution vs. time for three consecutive additions. Almost full conversion, consistent with the stoichiometry limit of added CAN, was attained after the first and second additions. However, TOF$_{50}$ in the second addition (348 min^{-1}) is significantly lower than that attained in the first measurement (726 min^{-1}). However, the largest difference was observed in the third addition of sacrificial oxidant, which afforded a lower conversion value (76%) in comparison with the 98% conversion achieved in the first and second additions (see ESI†). The decrease of TOF$_{50}$ values along the step-wise additions indicates partial loss of the catalytic activity that can be attributed to catalyst deactivation along time.[34b] It should be noted that only the first test showed an induction period of roughly 1 minute. The absence of a lag phase upon re-oxidation processes suggests that the pre-catalyst is
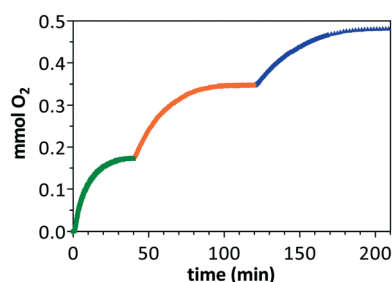

Plot with y-axis "mmol O$_2$" and x-axis "time (min)"

Fig. 5 Multi-step CAN-driven water oxidation catalysis by [Cp* IrCl{(MeIm)$_2$CHCOO}] (**1**). Oxygen production following the step-wise addition of 0.70 mmol of Ce(IV) to an initial 0.43 mM solution of **1** (2.5 mL, pH = 1.0) at 300 K.
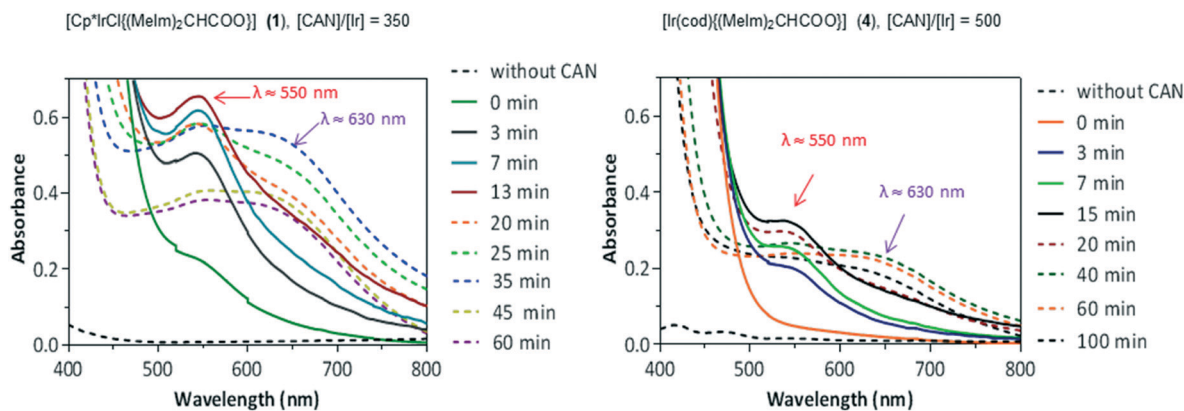
This journal is © The Royal Society of Chemistry 2019

Catal. Sci. Technol., 2019, **9**, 1437–1450 | **1443**

Fig. 6 Time evolution of the UV/vis spectra of solutions of catalyst precursors **1** (0.25 mM) and **4** (0.15 mM) after addition of CAN.

fully transformed into the active species after the first catalytic run.

Water oxidation catalysis: UV-vis studies

Time-course UV/vis spectroscopic studies under catalytic conditions were conducted with the aim to identify the nature of the water oxidation catalytic active species. Variable amounts of solid CAN were added to a solution of complex **1** (0.25 mM) in acidic water (0.1 M HNO₃, pH = 1) with [CAN]/[Ir] ratios in the range from 20–500. The addition of the sacrificial oxidant immediately led to an increase in the baseline spectra due to the formation of $O_2(g)$ bubbles. Regardless of the amount of added CAN, an absorption band at $\lambda \approx 550$ nm appeared at short reaction times reaching a maximum of intensity after 13 min. From that point, the intensity of this absorption band decreased while a new band appeared at $\lambda \approx 630$ nm as a broad shoulder (Fig. 6). Grotjahn et al. ascribed a band at 550 nm to the possible formation of IrO_x nanoparticles, which show an absorption band within this spectral region.[14b] However, an absorption band at $\lambda \approx 580$ nm was also attributed by Crabtree et al. to d–d transitions of octahedral iridium(IV) intermediates.[36] In fact, based on Crabtree's proposal, many authors have attributed this absorption band to the presence of iridium(IV) species rather than the formation of nanoparticles.[10a,32,37]

The recorded UV/vis spectra after the addition of CAN to a buffered water solution (0.1 M HNO₃, pH = 1) of catalyst precursor **4** (0.15 mM) with a [CAN]/[Ir] ratio of 500 are also shown in Fig. 6. Remarkably, under catalytic conditions both catalytic systems **1**/CAN and **4**/CAN exhibit similar absorption bands in the UV/vis spectra ($\lambda \approx 550$ and 630 nm).

The catalytic systems **1**/NaIO₄ and **4**/NaIO₄ were also investigated by UV/vis spectroscopy. The recorded spectra after the addition of solid NaIO₄ to degassed aqueous solution of **1** or **4** (0.25 and 0.15 mM, respectively) with [NaIO₄]/[Ir] ratios in the range of 20–500 closely resemble each other. Fig. 7 shows the time evolution of the UV/vis spectra using a [NaIO₄]/[Ir] ratio of 100. An absorption band at $\lambda \approx 585$ nm, reaching a maximum after 90 minutes, was observed for the catalytic system **1**/NaIO₄. In the case of the catalytic system **4**/NaIO₄ a weak absorption band appeared at $\lambda \approx 595$ nm together with a broad shoulder at $\lambda \approx 420$ nm. However, a new band at $\lambda \approx 585$ nm emerged after 10 minutes reaching a maximum absorbance after 60 minutes, which remains after 120 minutes.[37a]

The similarity of the UV/vis spectra for the catalytic systems based on both catalyst precursors (**1** and **4**) with the same sacrificial oxidant (CAN or NaIO₄) points to the participation of the same species in both catalytic systems. Furthermore, the active species participating in the periodate- and CAN-based catalytic systems should be closely related but
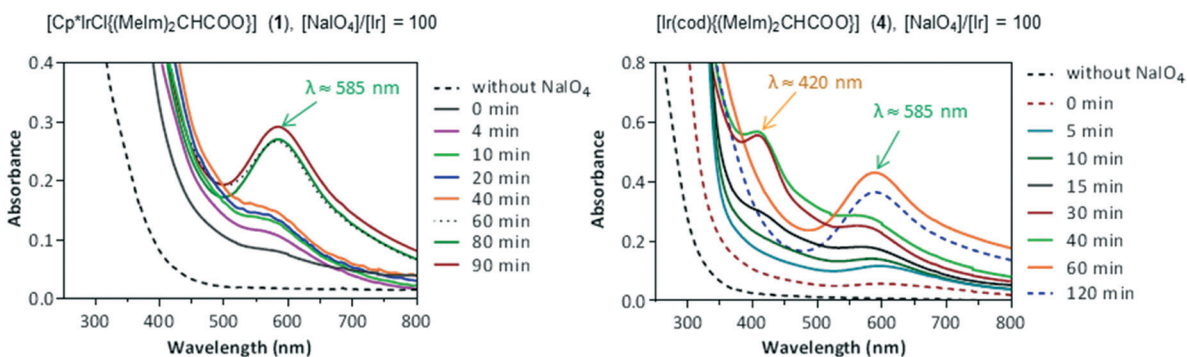

Fig. 7 Time evolution of the UV/vis spectra of solutions of catalyst precursors **1** (0.25 mM) and **4** (0.15 mM) after addition of NaIO₄.

1444 | Catal. Sci. Technol., 2019, **9**, 1437–1450

This journal is © The Royal Society of Chemistry 2019

different. In fact, time-course experiments revealed similar oxygen evolution profiles for both catalyst precursors. The overlay of the $O_2(g)$ evolution *vs.* time plots at the same concentration for both catalyst precursors showed comparable profiles for both sacrificial oxidants although a markedly shifted profile for catalyst precursor **4** using CAN as sacrificial oxidant at low catalyst concentrations (0.19 mM) is observed (Fig. 8). This shift is, in part, a consequence of the different lag phase although a lower catalytic activity for **4** under these conditions is also evident from the slope of both graphics at short reaction times.

These results together with the lag phase observed at the beginning of the catalytic reactions suggest that the Cp* and cod ligands might be degraded in route to the generation of the active species, similarly to the observed by Crabtree *et al.* in related Cp*Ir[III] and Ir[I](cod) complexes featuring 2-(2-pyridyl)-2-propanolate ligands.[37a]

In fact, the GC-MS spectra of the gas phase in the microreactor headspace after water oxidation catalysis by the systems **1**/CAN and **4**/CAN showed the presence of a small peak at *m/z* 44 corresponding to CO_2 traces which was attributed to the degradation of the hydrocarbon ligands (see ESI†). However, the degradation of the functionalized bis-NHC ligand followed by formation of IrO$_x$ (iridium oxide) nanoparticles cannot be excluded.[37a]

Dynamic light scattering studies

In order to investigate the possible formation of nanoparticles along water oxidation catalysis, dynamic light scattering (DLS) experiments were performed at different oxidant/catalyst ratios.[10a,36,37a] Interestingly, no nanoparticles were detected in solutions from the reaction of **1** and **4** neither using CAN nor NaIO$_4$ at [oxidant]/[Ir] ratios of 100, 650 and 1200 after standing for prolonged times. These results indicate that if nanoparticles are formed, the concentration must be below the detection limit of the technique (0.1 ppm) and the sizes must be smaller than 1 nm (see ESI†). In contrast, when IrCl$_3$ was employed as water oxidation catalyst using CAN and NaIO$_4$ as sacrificial oxidants, with a [oxidant]/[Ir] ratio of 100, DLS analysis of the dark brown and dark green solutions obtained after 30 minutes revealed the existence of nanoparticles of 400 and 99 nm sizes, respectively (see ESI†). Literature reports on iridium nanoparticles and

nanoclusters are generally characterized by their persistence along time, as it has been found in the case of IrCl$_3$, which is in agreement with formation of IrO$_x$ particles. These results suggest that water oxidation by catalyst precursors **1** and **4** proceeds in homogeneous phase.[37]

NMR studies

The oxidation of complexes **1** and **4** was also investigated by ^{1}H NMR spectroscopy with the aim of identifying possible species generated in the pre-catalysts activation step. The NMR experiments were conducted in *ca.* 60 mM catalyst solutions in D$_2$O (pH = 7) at room temperature. The consecutive addition of increasing amounts of sacrificial oxidant, CAN or NaIO$_4$, led to evolution of $O_2(g)$ bubbles that made difficult to homogenize the magnetic field. Nevertheless, ^{1}H NMR spectra were recorded under these conditions to identify possible species derived from the oxidative transformation of the catalyst precursors. PRESAT experiments were carried out in some cases in order to minimize the residual solvent signal.

The ^{1}H NMR spectrum of [Cp*IrCl{(MeIm)$_2$CHCOO}] (**1**) in D$_2$O showed the expected set of resonances for the functionalized bis-NHC ligand at δ 7.44, 7.38 (=CH) and 5.94 (CH) ppm. The addition of 2 equiv. of CAN to a yellow solution of **1** produced a darkening of the solution and the incipient appearance of two singlets at δ 8.26 and 2.11 ppm which correspond to formic acid[38] and acetic acid,[27b,37a] respectively. Increasing the amount of added CAN to 15 equiv. resulted in a dark blue solution with oxygen evolution whose ^{1}H NMR spectrum evidenced a decrease of the amount **1**, an increase of intensity of the formic and acetic acid resonances, and the appearance of a 1:1:1 signal at δ 6.68 ppm with a coupling constant J_{H-N} = 52.4 Hz corresponding to the NH$_4^+$ coming from CAN (see ESI†). Similarly, the ^{1}H NMR spectrum of the dark green solution obtained after addition of 10 equiv. of NaIO$_4$ also showed the presence of formic acid and acetic acid. The intensity of both resonances increased upon addition of NaIO$_4$ with concomitant decrease of those of **1** (see ESI†).

The ^{1}H NMR spectrum of a dark red solution of [Ir(cod){(MeIm)$_2$CHCOO}] (**4**) in D$_2$O (pH = 7) prior the addition of NaIO$_4$ showed the expected pattern of resonances at δ 7.43, 7.17, 6.44 (bis-NHC), and 4.83, 4.45 (=CH, cod) ppm (red circles, Fig. 9a). The addition of 2 equiv. of NaIO$_4$ produced an instantaneous colour change to green although not $O_2(g)$ bubbles were observed. However, the addition of 2 more equiv. afforded a deep green solution along with $O_2(g)$ evolution which turned into dark blue after addition of 10 equiv. of NaIO$_4$. The ^{1}H NMR of these solutions showed the clean formation of a new species featuring three resonances for the functionalized bis-NHC ligand at δ 7.67, 7.28 and 6.88 ppm, and two resonances for the =CH olefin protons of the cod ligand at δ 6.64 and 5.96 ppm (green circles), both largely downfield shifted compared to those of **4**. In particular, the shift of CHCOO resonance up to δ 6.88 ppm is a diagnostic for the κ^3-C,C′,O coordination of the carboxylate-
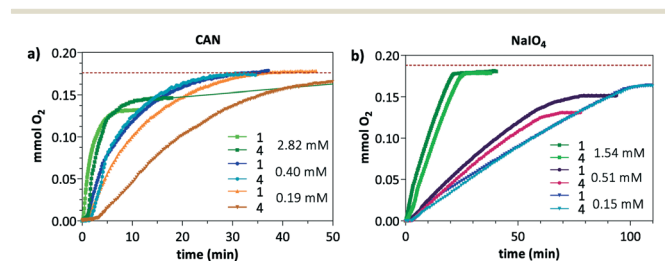

Fig. 8 Plots of $O_2(g)$ evolution *vs.* time at various concentrations of complexes **1** and **4** using: a) CAN (0.283 M) and b) NaIO$_4$ (0.154 M) as sacrificial oxidant.
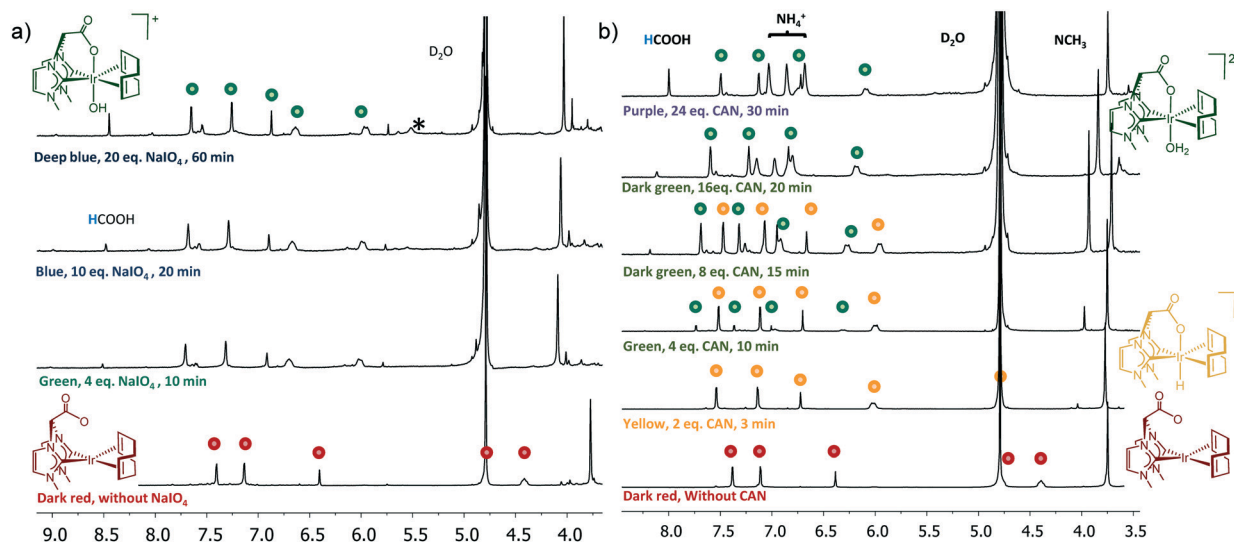
This journal is © The Royal Society of Chemistry 2019

Catal. Sci. Technol., 2019, **9**, 1437–1450 | **1445**

Fig. 9 Evolution of the ^{1}H NMR spectra (D$_2$O, pH = 7, 298 K) of a solution of [Ir(cod){(MeIm)$_2$CHCOO}] (**4**) (60 mM) after consecutive additions of: a) solid NaIO$_4$, and b) solid CAN (* 1,5-cyclooctadiene).

functionalized bis-NHC ligand.[16] The observed chemical shifts compares well with those of the cation [IrCl(cod)κ^3-C,C′,O-{(MeIm)$_2$CHCOO}]$^+$ which binds an electronegative ligand *trans* to the carboxylate moiety. Thus, the spectroscopic data are compatible with the formation of an Ir(III) octahedral species [IrX(cod){(MeIm)$_2$CHCOO}]$^{n+}$ with a O-donor ligand *trans* to the carboxylate fragment. This species has been prepared by reaction of **4** with one equiv. of NaIO$_4$ in water and characterized as the hydroxo complex [Ir(OH)(cod){(MeIm)$_2$CHCOO}][IO$_3$] (**8**). Compound **8** has been isolated as a sparingly soluble white solid in 63% yield and characterized by ^{1}H NMR and HRESI-MS (see Experimental section and ESI†). The stability of this species under the reaction conditions is remarkable. The addition of an overall of 20 equiv. resulted in the formation of only trace amounts of formic acid (δ 8.45 ppm) and free 1,5-cyclooctadiene (δ 5.50 and 2.30 ppm) after 60 min. However, an increase in the amount of formic acid with concomitant decrease of that of **8** was observed after the addition of more NaIO$_4$ which indicates the steady transformation of **8** into the catalytic active species.

This spectroscopic study was also extended to the catalytic system **4**/CAN (Fig. 9b). The addition of 2 equiv. of CAN to an aqueous dark red solution of **4** in D$_2$O (pH = 7) resulted in a colour change to yellow along with O$_2$(g) evolution. The ^{1}H NMR spectrum of this solution showed the presence of a single species featuring three resonances at δ 7.54, 7.14 and 6.72 ppm for the bis-NHC ligand and two resonances for the =CH protons of the cod ligand at δ 6.01 and 4.76 ppm (yellow circles). The addition of 2 more equiv. of CAN afforded a green solution as a consequence of the formation of a new species exhibiting the characteristic resonances for the bis-NHC (δ 7.73, 7.37 and 7.01 ppm) and cod (δ 6.97 and 6.31 ppm) ligands (green circles). A κ^3-C,C′,O coordination of the carboxylate-functionalized bis-NHC ligand is inferred for both species owing to the remarkable downfield shifted CHCOO

resonance compared to **4**. The yellow species is progressively transformed into the green one upon addition of CAN, which is the only observed species after addition of 16 equiv. of CAN. Subsequent addition of CAN resulted in a colour change to purple, through dark green, with steady O$_2$(g) evolution. After addition of 24 equiv. of CAN, the species labelled in green is still observed although masked by the characteristic 1:1:1 resonance at δ 6.86 ppm with ($J_{H–N}$ = 52.1 Hz) corresponding to the NH$_4^+$ coming from CAN. The ^{1}H NMR spectra also revealed the presence of formic acid (δ 8.00 ppm).

The species denoted with yellow circles has been identified as the deuterido [IrD(cod){(MeIm)$_2$CHCOO}]$^+$ (*d*-**9**) complex by comparison with the ^{1}H NMR of a sample obtained by protonation of **4** with triflic acid in D$_2$O.[17] Thus, the acid media provided by the hydrolysis of Ce^{4+} in D$_2$O is responsible for the protonation of **4**. Although the chemical shifts of the resonances for the species labelled in green are not strictly comparable with those of **8** the spectroscopic data also point to a species also having an O-donor ligand trans to the carboxylate moiety. We hypothesize that the first oxidation product resulting from the oxidation of **4** is strongly dependent of the pH of the reaction media. Thus, the formation of the hydroxo-Ir(III) species [Ir(OD)(cod){(MeIm)$_2$CHCOO}]$^+$ (**8**) results from the oxidation of **4** in neutral medium (IO$_4^-$), whereas the aqua-Ir(III) species [Ir(D$_2$O)(cod){(MeIm)$_2$-CHCOO}]$^{2+}$ (**10**) might be formed in acidic medium (CAN) (Fig. 10). This species has independently prepared by protonation of **8** in water (HNO$_3$) and isolated in low yield as colourless solid which has been characterized by ^{1}H NMR and HRESI-MS (see Experimental section and ESI†).

The reactivity of **4** with CAN has been also studied at pH = 1 (D$_2$O, HNO$_3$ 0.1 M) affording similar results. As expected, compound **4** is completely protonated at pH = 1 to afford the hydrido species **9**. However, the step-wise addition of solid

1446 | *Catal. Sci. Technol.*, 2019, **9**, 1437–1450

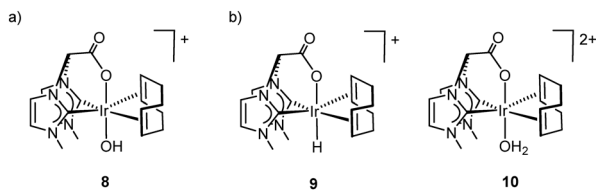This journal is © The Royal Society of Chemistry 2019

Fig. 10 Observed species (^{1}H NMR, D_2O) in the oxidation of **4** with IO_4^- (a) and CAN (b) (the corresponding deuterated species are formed under the reaction conditions).

CAN showed that the conversion **9** → **10** → active species, is much faster under this conditions (see ESI†).

The transformation of the hydrido compound **9** into the aquo species **10** should follow an oxidative pathway. Then, two electron oxidation of **9** by two equiv. of CAN might afford the intermediate iridium(v)-hydride species from which the acidic hydride ligand is easily transferred to water to give **10** (Scheme 1). Although protonation of **9** with release of molecular hydrogen and concomitant coordination of H_2O could be an alternative route for the formation **10**, compound **9** remains unchanged at pH 1 for four hours which rule out this pathway.

Mass spectrometric studies

The ESI-MS spectra of aqueous solutions of [Cp* IrCl{(MeIm)$_2$CHCOO}] (**1**) and [(cod)Ir{(MeIm)$_2$CHCOO}] (**4**) showed peaks at m/z 583.15 and 521.15, respectively, that correspond to the protonated molecular ions $[M + H]^+$. In addition, the ESI-MS spectrum of **1** showed two peaks at m/z 547.17 and 503.18 for the ions $[1-Cl]^+$ and $[1-Cl–CO_2]^+$, respectively (see ESI†). The addition of CAN to *ca.* 1×10^{-3} mM water solutions (pH = 7) of the catalyst precursors resulted in oxygen evolution and the immediate formation of new peaks in the MS spectra. However, at low CAN/Ir ratios the molecular ions were still detected at least 24 h after CAN addition, whereas at high CAN/Ir ratios poor MS spectra were obtained due to the blinding of the detector both in ESI$^+$ and MaldiToF modes.

The MS-ESI$^+$ spectrum of a water solution of **1** after the addition of 50 equiv. of CAN, measured after 5 min when oxygen is evolving from the sample, showed three main species at m/z 597.11, 553.15 and 519.15, which showed the right isotopic pattern for the ions $[1 + O]^+$, $[1-CO_2 + O]^+$ and $[1-CO_2–Cl + O + H]^+$ (Fig. 11a). These species were not observed in the MS-ESI$^+$ spectrum recorded after 24 h that only showed the
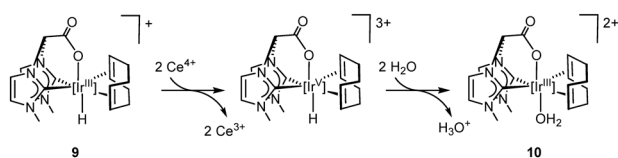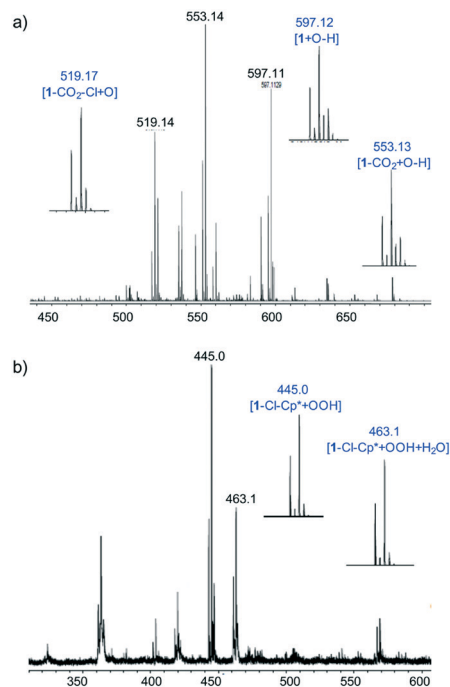

Fig. 11 Mass spectra of water solutions of **1** (pH = 7) treated with 50 equiv. of CAN recorded after 5 min: a) MS-ESI$^+$ spectrum, b) MS-MaldiToF spectrum. The insets show the simulated isotopic patterns for the identified peaks.

peak for $[1 + H]^+$. The MS-MaldiToF spectrum of after the addition of 50 equiv. of CAN showed two mains peaks at m/z 463.2 and 445.0 whose isotopic distribution agreed with that of the ions $[1-Cl–Cp^* + OOH + H_2O]$ and $[1-Cl–Cp^* + OOH]$, respectively (Fig. 11b).

The MS-ESI$^+$ spectrum of a water solution of the iridium(I) complex **4** treated with 50 equiv. of CAN recorded after 10 min showed two main peaks at m/z 519.11 and 537.12, with the right isotopic pattern for the ions $[4 − H]^+$ and $[4 + H + O]^+$. After standing the solution for 24 h a similar MS-ESI$^+$ spectrum was observed. The MS-MaldiToF spectrum after 24 h showed two peaks at m/z 521.1 and 599.1, that correspond to the protonated molecular ion $[4 + H]^+$ and the ion $[4 + H + O + NO_3]^+$ (see ESI†). Unfortunately, despite the efforts made by using a range of CAN/Ir ratios, we have failed to detect any cod-free bis-NHC/Ir species in this case.

The observation of hydroperoxo species derived from $[Ir\{(MeIm)_2CHCOO\}(OOH)(H_2O)_x]^+$ in the MS spectra of the catalytic system **1**/CAN is a clue for the possible participation of high-valent iridium intermediates stabilized by the carboxylate-functionalized bis-NHC ligand. On the other hand, although the oxidative degradation of Cp* and cod ligands could be anticipated in view of the spectroscopic evidences, the nature of the oxygen-containing species observed in the MS spectra cannot be determined reliably. In this regard, Macchioni *et al.* have recently shown that the mechanism for the degradation of the Cp* ancillary ligand in iridium-based water oxidation catalysts consists on a multistep oxidative process in which Cp*Ir^{III}-superoxo species

Scheme 1 Oxidative pathway for the transformation of the hydrido-Ir(III) complex into the aquo-Ir(III) species.

This journal is © The Royal Society of Chemistry 2019

Catal. Sci. Technol., 2019, **9**, 1437–1450 | **1447**

play a key role.[38a] However, the degradation pathways for the cod ligand in Ir(cod)-based water oxidation catalysts are much less understood.[39,40]

Electrochemical studies

The redox behaviour of complexes **1** and **4**, without the chemical complications caused by chemical oxidants (CAN or NaIO$_4$) was investigated by cyclic voltammetry (CV) using 1 mM water solutions of the complexes. The cyclic voltammogram profile for **1** shows a poor resolved anodic peak at 1.70 V, a hardly visible wave at 0.91 V and an irreversible reduction peak at 0.27 V (Fig. 12a).

The CVs of water solutions of complex **1** (1.0 mM) at pH = 1.0 and 7.0 in the window 0.0 to 1.3 V are shown in Fig. 12b. The observed current increase at potentials over 1.2 V is assigned to the electrocatalytic water oxidation associated to **1** which is in accordance with the lower overpotentials required for electrochemically driven water oxidation.[41] The anodic response at 0.91 V at pH 7 is hardly observed at pH 1 whereas the irreversible reduction peak is shifted to 0.40 V. The oxidation peak at 0.91 V might be assigned to the Ir^{III}/Ir^{IV} redox couple. In fact, a linear relationship between the peak current (I) for the redox couple and the square root of the scan rate ($v^{1/2}$) was observed for scan rates in the range of 20–200 mV s^{-1} what is consistent with a rate-limiting step prior to electron transfer to the electrode.[42] A linear correlation has also been observed for the reduction peaks at 0.40 V and 0.25 V at pH 1 and 7, respectively (see ESI†).

The CV for the iridium(I) compound **4** in water showed a barely discernible irreversible oxidation peak at 0.54 V which is associate to reduction peak at 0.16 V. This couple is accompanied with a quasi-reversible redox couple at $\varepsilon_{1/2}$ = −0.44 V (Fig. 13). The analysis of this wave with a narrow scan win-
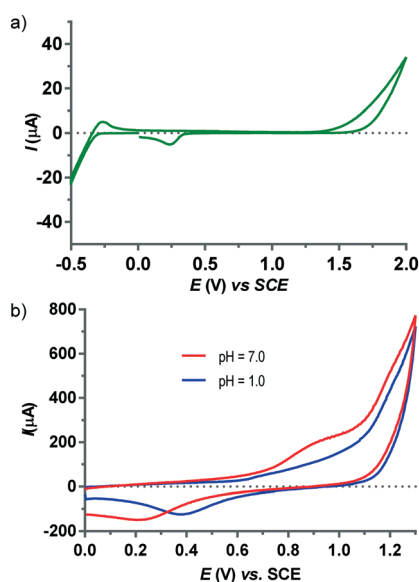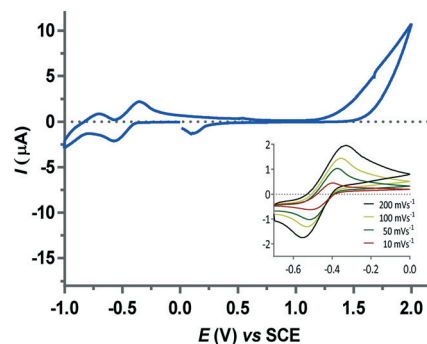

Fig. 13 CV for compound **4** in water at pH 7. Inset: CVs of the quasi-reversible wave centred at $\varepsilon_{1/2}$ = −0.44 V at different scan rates.

dow and scan rates varying from 10 to 200 mV s^{-1} roughly fulfils the standard reversibility criteria. In particular, the ratio of cathodic/anodic peak currents (I_{pc}/I_{pa}), that is expected to be unity for an ideal reversible process, is found to be 1.04, and the current function $I(v)^{1/2}$ (v = scan rate) is approximately constant. However, the peak separation (ΔE_p) of 129 mV is slightly larger than the ideal value for a reversible wave (59 mV). This electrochemical process is tentatively assigned to the redox couple Ir^{II}/Ir^{I} whereas the irreversible wave might correspond to the Ir^{III}/Ir^{II} redox couple.[43] Unfortunately, the easy protonation of compound **4** in acidic medium prevents to study the pH influence in the redox behaviour.

4. Conclusions

Zwitterionic water-soluble [Cp*Ir^{III}Cl{(MeIm)$_2$CHCOO}] and [IrI(cod){(MeIm)$_2$CHCOO}] complexes having a carboxylate bridge-functionalized bis-NHC ligand have shown to be effective water oxidation catalysts using chemical oxidants such as CAN or NaIO$_4$. Excellent yields and TOF$_{50}$ numbers up to 1000 h^{-1} have been achieved when using [CAN]/[Ir] ratios higher than 700. Regardless of the oxidant employed, both catalyst precursors provided similar oxygen evolution profiles with short induction periods. This lag phase is slightly longer for the catalyst precursor [Ir^{I}(cod){(MeIm)$_2$CHCOO}]. Changes in the wingtips of the bis-NHC ligand or in the catalyst framework did not improve the catalytic performance of the zwitterionic complex [Cp*Ir^{III}Cl{(MeIm)$_2$CHCOO}].

Kinetic, spectroscopic and DLS studies carried out with both catalysts precursors suggest the participation of common homogeneous high-valent iridium intermediate species in water oxidation catalysis. In particular, the resemblance of the UV/vis spectra and the similarity of the oxygen evolution profiles at moderate oxidant/catalyst ratios for both catalyst precursors and the same chemical oxidant, point to the likely degradation of the hydrocarbon ligands, Cp* and cod, in the pre-catalyst activation step. NMR spectroscopic studies at low oxidant/catalyst ratios have provided some hints on the pre-catalyst activation processes. In the case of [Cp*Ir^{III}Cl{(MeIm)$_2$CHCOO}] formic and acetic acids were immediately formed regardless of the sacrificial oxidant employed.

Fig. 12 a) CV for **1** in water at pH = 7, b) pH-dependent CVs of complex **1** in aqueous solution (scan rate 200 mV s^{-1}).

However, in the case of $[Ir^I(cod)\{(MeIm)_2CHCOO\}]$, three different iridium(III) species stabilized by the tridentate coordination of the functionalized bis-NHC ligand have been identified, together with the formation of formic acid.

Taking all these results together, the molecular species responsible for water oxidation should be stabilized by the bis-NHC ligand, although the presence of the carboxylate function under the reaction conditions could be a subject of debate. Evidence for this hypothesis comes from the observation in the MS spectra of the reaction of 1 with CAN of hydroperoxo species derived from $[Ir\{(MeIm)_2CHCOO\}(OOH)(H_2O)_x]^+$. Based on these evidences, a mechanism involving high-valent $Ir^{III}/Ir^{IV}/Ir^V$ intermediate species stabilized by the carboxylate functionalized bis-NHC ligand, similar to those proposed by Crabtree[13c,32] and Reek[44] for Cp*Ir(III) catalysts, could be operative.

Conflicts of interest

There are no conflicts to declare.

Acknowledgements

Notes and references

1 (a) P. Sutra and A. Igau, Curr. Opin. Green Sustain Chem., 2018, 10, 60–67; (b) N. Armaroli and V. Balzan, Chem. – Eur. J., 2016, 22, 32–57.

2 (a) D. G. Nocera, Acc. Chem. Res., 2012, 45, 767–776; (b) Y. Jia, Y. Xu, R. Nie, F. Chen, Z. Zhu, J. Wang and H. Jing, J. Mater. Chem. A, 2017, 5, 5495–5501; (c) R. Razeghifard, in Natural and Artificial Photosynthesis: Solar Power as an Energy Source, Wiley, Hoboken, New Jersey, 2013.

3 (a) J. D. Blakemore, R. H. Crabtree and G. W. Brudvig, Chem. Rev., 2015, 115, 12974–13005; (b) M. D. Karkas, O. Verho, E. V. Johnston and B. Akermark, Chem. Rev., 2014, 114, 11863–12001; (c) A. Llobet, in Molecular Water Oxidation Catalysis: A Key Topic for New Sustainable Energy Conversion Schemes, Wiley, United Kingdom, 2014; (d) I. Roger, M. A. Shipman and M. D. Symes, Nat. Rev. Chem., 2017, 1, 0003.

4 (a) A. Petronilho, M. Rahman, J. A. Woods, H. Al-Sayyed, H. Müller-Bunz, J. M. D. MacElroy, S. Bernhard and M. Albrecht, Dalton Trans., 2012, 41, 13074–13080; (b) R. Bofill, J. García-Antón, L. Escriche and X. Sala, J. Photochem. Photobiol., B, 2015, 152, 71–81.

5 A. R. Parent, R. H. Crabtree and G. W. Brudvig, Chem. Soc. Rev., 2013, 42, 2247–2252.

6 (a) S. W. Gersten, G. J. Samuels and T. J. Meyer, J. Am. Chem. Soc., 1982, 104, 4029–4030; (b) J. A. Gilbert, D. S. Eggleston, W. R. Murphy, D. A. Geselowitz, S. W. Gersten, D. J. Hodgson and T. J. Meyer, J. Am. Chem. Soc., 1985, 107, 3855–3864.

7 (a) L. Duan, L. Wang, F. Li, F. Li and L. Sun, Acc. Chem. Res., 2015, 48, 2084–2096; (b) J. Creus, R. Matheu, I. Peñafiel, D. Moonshiram, P. Blondeau, J. Benet-Buchholz, J. García-Antón, X. Sala, C. Godard and A. Llobet, Angew. Chem., Int. Ed., 2016, 55, 15382–15386; (c) L. Duan, F. Bozoglian, S. Mandal, B. Stewart, T. Privalov, A. Llobet and L. Sun, Nat. Chem., 2012, 4, 418–423.

8 N. D. McDaniel, F. J. Coughlin, L. L. Tinker and S. Bernhard, J. Am. Chem. Soc., 2008, 130, 210–217.

9 (a) J. F. Hull, D. Balcells, J. D. Blakemore, C. D. Incarvito, O. Eisenstein, G. W. Brudvig and R. H. Crabtree, J. Am. Chem. Soc., 2009, 131, 8730–8731; (b) A. Bucci, G. Menendez Rodriguez, G. Bellachioma, C. Zuccaccia, A. Poater, L. Cavallo and A. Macchioni, ACS Catal., 2016, 6, 4559–4563; (c) A. Savini, G. Bellachioma, G. Ciancaleoni, C. Zuccaccia, D. Zuccaccia and A. Macchioni, Chem. Commun., 2010, 46, 9218–9219; (d) J. DePasquale, I. Nieto, L. E. Reuther, C. J. Herbst-Gervasoni, J. J. Paul, V. Mochalin, M. Zeller, C. M. Thomas, A. W. Addison and E. T. Papish, Inorg. Chem., 2013, 52, 9175–9183; (e) M. Navarro, M. Li, H. Müller-Bunz, S. Bernhard and M. Albrecht, Chem. – Eur. J., 2016, 22, 6740–6745; (f) O. Diaz-Morales, T. J. P. Hersbach, D. G. H. Hetterscheid, J. N. H. Reek and M. T. M. Koper, J. Am. Chem. Soc., 2014, 136, 10432–10439; (g) A. Lewandowska-Andralojc, D. E. Polyansky, C.-H. Wang, W.-H. Wang, Y. Himeda and E. Fujita, Phys. Chem. Chem. Phys., 2014, 16, 11976–11987.

10 (a) Z. Codolà, J. M. S. Cardoso, B. Royo, M. Costas and J. Lloret-Fillol, Chem. – Eur. J., 2013, 19, 7203–7213; (b) T. P. Brewster, J. D. Blakemore, N. D. Schley, C. D. Incarvito, N. Hazari, G. W. Brudvig and R. H. Crabtree, Organometallics, 2011, 30, 965–973; (c) D. G. H. Hetterscheid and J. N. H. Reek, Chem. Commun., 2011, 47, 2712–2714.

11 R. Lalrempuia, N. D. McDaniel, H. Müller-Bunz, S. Bernhard and M. Albrecht, Angew. Chem., Int. Ed., 2010, 49, 9765–9768.

12 J. Graeupner, U. Hintermair, D. L. Huang, J. M. Thomsen, M. Takase, J. Campos, S. M. Hashmi, M. Elimelech, G. W. Brudvig and R. H. Crabtree, Organometallics, 2013, 32, 5384–5390.

13 (a) A. Macchioni, Eur. J. Inorg. Chem., 2019, 7–17; (b) B. Mahanti, G. González, E. Martínez-Castro, M. Bedin, B. Martín-Matute, S. Ott and A. Thapper, ChemSusChem, 2017, 10, 4616–4623; (c) J. M. Thomsen, D. L. Huang, R. H. Crabtree and G. W. Brudvig, Dalton Trans., 2015, 44, 12452–12472; (d) I. Corbucci, A. Macchioni and M. Albrecht, in Iridium Complexes in Water Oxidation Catalysis in Iridium Optoelectronic and Photonics Applications, ed. J. E. Zysman-Colman, John Wiley & Sons Ltd., 2017, pp. 617–654.

14 (a) G. Menendez Rodriguez, G. Gatto, C. Zuccaccia and A. Macchioni, ChemSusChem, 2017, 10, 4503–4509; (b) D. B. Grotjahn, D. B. Brown, J. K. Martin, D. C. Marelius, M.-C. Abadjian, H. N. Tran, G. Kalyuzhny, K. S. Vecchio, Z. G. Specht, S. A. Cortes-Llamas, V. Miranda-Soto, C. van

This journal is © The Royal Society of Chemistry 2019

Catal. Sci. Technol., 2019, 9, 1437–1450 | 1449

Niekerk, C. E. Moore and A. L. Rheingold, *J. Am. Chem. Soc.*, 2011, **133**, 19024–19027; (*c*) S. E. Castillo-Blum, D. T. Richens and A. G. Sykes, *Inorg. Chem.*, 1989, **28**, 954–960; (*d*) D. A. Pankratov, P. N. Komozin and Y. M. Kiselev, *Russ. J. Inorg. Chem.*, 2011, **56**, 1794–1799; (*e*) H. Junge, N. Marquet, A. Kammer, S. Denurra, M. Bauer, S. Wohlrab, F. Gartner, M.-M. Pohl, A. Spannenberg, S. Gladiali and M. Beller, *Chem. – Eur. J.*, 2012, **18**, 12749–12758; (*f*) A. R. Parent, T. P. Brewster, W. de Wolf, R. H. Crabtree and G. W. Brudvig, *Inorg. Chem.*, 2012, **51**, 6147–6152.

15 R. Pokhrel, M. K. Goetz, S. E. Shaner, X. Wu and S. S. Stahl, *J. Am. Chem. Soc.*, 2015, **137**, 8384–8387.

16 R. Puerta-Oteo, M. V. Jiménez, F. J. Lahoz, F. J. Modrego, V. Passarelli and J. J. Pérez-Torrente, *Inorg. Chem.*, 2018, **57**, 5526–5543.

17 R. Puerta-Oteo, M. V. Jiménez, F. J. Lahoz, F. J. Modrego, V. Passarelli and J. J. Pérez-Torrente, *Organometallics*, 2018, **37**, 684–696.

18 *Purification of Laboratory Chemicals*, ed. W. L. F. Armarego and C. L. L. Chai, Butterworth-Heinemann, Oxford, 6th edn, 2009.

19 C. White, A. Yates, P. M. Maitlis and D. M. Heinekey, *Inorg. Synth.*, 1992, **29**, 228–234.

20 M. A. Bennett, T.-N. Huang, T. W. Matheson and A. K. Smith, *Inorg. Synth.*, 1982, **21**, 74–79.

21 M. Vogt, V. Pons and D. M. Heinekey, *Organometallics*, 2005, **24**, 1832–1836.

22 www.manonthemoontech.com.

23 M. Li, K. Takada, J. I. Goldsmith and S. Bernhard, *Inorg. Chem.*, 2016, **55**, 518–526.

24 Z. Codolà, L. Gomez, S. T. Kleespies, L. Que, M. Costas and J. Lloret-Fillol, *Nat. Commun.*, 2015, **6**, 5865–5874.

25 I. Corbucci, A. Petronilho, H. Müller-Bunz, L. Rocchigiani, M. Albrecht and A. Macchioni, *ACS Catal.*, 2015, **5**, 2714–2718.

26 A. Bucci, A. Savini, L. Rocchigiani, C. Zuccaccia, S. Rizzato, A. Albinati, A. Llobet and A. Macchioni, *Organometallics*, 2012, **31**, 8071–8074.

27 (*a*) A. Savini, A. Bucci, G. Bellachioma, L. Rocchigiani, C. Zuccaccia, A. Llobet and A. Macchioni, *Eur. J. Inorg. Chem.*, 2014, 690–697; (*b*) A. Savini, P. Belanzoni, G. Bellachioma, C. Zuccaccia, D. Zuccaccia and A. Macchioni, *Green Chem.*, 2011, **13**, 3360–3374.

28 D. Hong, M. Murakami, Y. Yamada and S. Fukuzumi, *Energy Environ. Sci.*, 2012, **5**, 5708–5716.

29 A. R. Parent, T. P. Brewster, W. De Wolf, R. H. Crabtree and G. W. Brudvig, *Inorg. Chem.*, 2012, **51**, 6147–6152.

30 A. Volpe, A. Sartorel, C. Tubaro, L. Meneghini, M. Di Valentin, C. Graiff and M. Bonchio, *Eur. J. Inorg. Chem.*, 2014, 665–675.

31 A. Lewandowska-Andralojc, D. Polyansky, C.-H. Wang, W.-H. Wang, Y. Himeda and E. Fujita, *Phys. Chem. Chem. Phys.*, 2014, **16**, 11976–11987.

32 J. D. Blakemore, N. D. Schley, D. Balcells, J. F. Hull, G. W. Olack, C. D. Incarvito, O. Eisenstein, G. W. Brudvig and R. H. Crabtree, *J. Am. Chem. Soc.*, 2010, **132**, 16017–16029.

33 D. G. Blackmond, *Angew. Chem., Int. Ed.*, 2005, **44**, 4302–4320.

34 (*a*) J. M. Koelewijn, M. Lutz, W. I. Dzik, R. J. Detz and J. N. H. Reek, *ACS Catal.*, 2016, **6**, 3418–3427; (*b*) J. A. Woods, R. Lalrempuia, A. Petronilho, N. D. McDaniel, H. Müller-Bunz, M. Albrecht and S. Bernhard, *Energy Environ. Sci.*, 2014, **7**, 2316–2328.

35 A. Ikeda-Ohno, S. Tsushima, C. Hennig, T. Yaita and G. Bernhard, *Dalton Trans.*, 2012, **41**, 7190–7192.

36 U. Hintermair, S. M. Hashmi, M. Elimelech and R. H. Crabtree, *J. Am. Chem. Soc.*, 2012, **134**, 9785–9795.

37 (*a*) U. Hintermair, S. W. Sheehan, A. R. Parent, D. H. Ess, D. T. Richens, P. H. Vaccaro, G. W. Brudvig and R. H. Crabtree, *J. Am. Chem. Soc.*, 2013, **135**, 10837–10851; (*b*) M. Zhou, D. Balcells, A. R. Parent, R. H. Crabtree and O. Eisenstein, *ACS Catal.*, 2012, **2**, 208–218.

38 (*a*) C. Zuccaccia, G. Bellachioma, O. Bortolini, A. Bucci, A. Savini and A. Macchioni, *Chem. – Eur. J.*, 2014, **20**, 3446–3456; (*b*) C. Wang, J.-L. Wang and W. Lin, *J. Am. Chem. Soc.*, 2012, **134**, 19895–19908.

39 (*a*) M. R. Kelley and J.-U. Rohde, *Dalton Trans.*, 2014, **43**, 527–537; (*b*) M. P. del Río, M. A. Ciriano and C. Tejel, *Angew. Chem., Int. Ed.*, 2008, **47**, 2502–2505; (*c*) B. de Bruin, M. J. Boerakker, J. A. Brands, J. J. J. M. Donners, M. P. J. Donners, R. de Gelder, J. M. M. Smits, A. W. Gal and A. L. Spek, *Chem. – Eur. J.*, 1999, **5**, 2921–2936.

40 (*a*) D. G. H. Hetterscheid, M. Bens and B. de Bruin, *Dalton Trans.*, 2005, 979–984; (*b*) D. G. H. Hetterscheid, M. Klop, R. J. N. A. M. Kicken, J. M. M. Smits, E. J. Reijerse and B. de Bruin, *Chem. – Eur. J.*, 2007, **13**, 3386–3405.

41 A. A. Schilt, *Anal. Chem.*, 1963, **35**, 1599–1602.

42 (*a*) P. Zanello, in *Inorganic Electrochemistry. Theory, Practice and Applications*, RSC, Cambridge, 2003; (*b*) J. M. Savéant, in *Elements of Molecular and Biomolecular Electrochemistry. An Electrochemical Approach to Electron Transfer Chemistry*, Wiley, Hoboken, New Jersey, 2006; (*c*) Z. Chen, J. J. Concepcion, H. Luo, J. F. Hull, A. Paul and T. J. Meyer, *J. Am. Chem. Soc.*, 2010, **132**, 17670–17673.

43 (*a*) M. P. García, M. V. Jiménez, L. A. Oro, F. J. Lahoz and P. J. Alonso, *Angew. Chem., Int. Ed. Engl.*, 1992, **31**, 1527–1529; (*b*) M. P. García, M. V. Jiménez, L. A. Oro, F. J. Lahoz, J. M. Casas and P. J. Alonso, *Organometallics*, 1993, **12**, 3257–3263.

44 A. Venturini, A. Barbieri, J. N. Reek and D. G. Hetterscheid, *Chem. – Eur. J.*, 2014, **20**, 5358–5368.

1450 | *Catal. Sci. Technol.*, 2019, **9**, 1437–1450

This journal is © The Royal Society of Chemistry 2019